JOURNAL OF GUIDANCE, CONTROL, AND DYNAMICS
Vol. 17, No. 5, September–October 1994

Case Study Comparison of Linear Quadratic Regulator and H_∞ Control Synthesis

James H. Vincent*
Control Applications, Inc., Marina, California 93933
Abbas Emami-Naeini†
Integrated Systems, Inc., Santa Clara, California 95054
and
Nasser M. Khraishi
Infinity Financial Technology, Inc., Mountain View, California 94043

The goal of this paper is to compare the relative strengths of linear quadratic and H_∞ multivariable control law synthesis techniques. Design application considerations for each approach are also offered. The context of this design comparison is the AIAA Design Challenge in Automatic Control. The linear quadratic regulator (LQR) and H_∞ approaches are compared through the design of lateral-directional control laws for a single-flight condition. Desired flying quality characteristics are implemented through the utilization of an explicit model-following flight control system. With the model-following control system, the pilot commands the desired response (i.e., lateral stick force is used to command roll rate, instead of aileron deflection). The control system design is based on the notion of generalized actuators and the use of a *control selector* to distribute commands to the redundant effectors.

Introduction

MANY multivariable control system design techniques have been developed over the last two decades. The purpose of the AIAA Design Challenge[1] is to apply some of these methods to a realistically complex aircraft control problem. The authors have developed their own philosophy for designing multivariable control laws through their participation in a number of aircraft and spacecraft multivariable control design programs over the last decade, which include DMICS,[2–4] OWRA,[5] the E-7D STOVL,[6] and the MAVRIC[7,8] programs. This philosophy has been to carry out point designs and to use gain scheduling to implement full flight envelope control systems. Explicit model-following multivariable control laws have been designed in each case. The explicit model embodies the desired aircraft response. A control structure has been developed that allows the marriage of the explicit model-following methodology with various multivariable control system design approaches such as the linear quadratic regulator (LQR) and H_∞. In the DMICS, OWRA, and E-7D STOVL programs LQR was used; whereas in MAVRIC an H_∞ explicit model-following technique was used. The marriage of the explicit model-following method with the LQR and recently with the H_∞ methods has been the cornerstone of our design approach. The freedom and the physical insight provided by the explicit model-following in the aerospace problems have been found to be very valuable. A common control structure provides the basis for the LQR and H_∞ designs. Developments in control theory have resulted in the emergence of powerful analysis techniques to deal with a variety of sources of modeling errors.[7,8] These analysis techniques are used to evaluate the designs and to provide comparisons of performance. This paper presents the specific design approach for both the LQR and H_∞ regulator design techniques along with an evaluation of the resulting control laws.

A lateral-directional control system design example is presented to illustrate general features of our design methodology and to provide a means for comparing the two regulator synthesis methods. All design work pertains to a single-flight condition: $M = 0.9$ and $h = 9800$ ft. The NASA Dryden nonlinear simulation model of the study aircraft[1] was trimmed at this flight condition, and a lateral-directional state-space model of the form shown in the following equation was generated:

$$\begin{aligned} \dot{x}_{ac} &= A_{ac}x_{ac} + B_{ac}u_{ac} \\ y_{ac} &= C_{ac}x_{ac} + D_{ac}u_{ac} \end{aligned} \tag{1a}$$

where

$$x_{ac} = \begin{bmatrix} v \\ P \\ R \\ \phi \end{bmatrix} \begin{bmatrix} \text{lateral velocity, fps} \\ \text{roll rate, rad/s} \\ \text{yaw rate, rad/s} \\ \text{bank angle, rad} \end{bmatrix} \tag{1b}$$

$$u_{ac} = \begin{bmatrix} \delta_A \\ \delta_D \\ \delta_R \end{bmatrix} \begin{bmatrix} \text{aileron, deg} \\ \text{differential tail, deg} \\ \text{rudder, deg} \end{bmatrix} \tag{1c}$$

$$y_{ac} = \begin{bmatrix} n_y \\ \dot{\beta} \\ P \\ R \\ \phi \\ \beta \end{bmatrix} \begin{bmatrix} \text{lateral acceleration, } g \\ \text{sideslip rate, deg/s} \\ \text{roll rate, deg/s} \\ \text{yaw rate, deg/s} \\ \text{bank angle, deg} \\ \text{sideslip, deg} \end{bmatrix} \tag{1d}$$

and

$$A_{ac} = \begin{bmatrix} -0.3591 & 43.7145 & -970.2958 & 32.1674 \\ -0.0924 & -3.3230 & 2.1789 & 0.0 \\ 0.0181 & -0.0670 & -1.0037 & 0.0 \\ 0.0 & 1.0000 & 0.0451 & 0.0 \end{bmatrix}$$

$$B_{ac} = \begin{bmatrix} 0.0 & -1.0135 & 0.9411 \\ 0.6922 & 1.0539 & 0.0555 \\ 0.1018 & 0.1238 & -0.1465 \\ 0.0 & 0.0 & 0.0 \end{bmatrix} \tag{1e}$$

Received March 6, 1992; revision received Oct. 12, 1993; accepted for publication Oct. 13, 1993.

*President. Member AIAA.

†Research Scientist.

$$C_{ac} = \begin{bmatrix} -0.0112 & 0.0 & 0.0 & 0.0 \\ -0.0212 & 2.5789 & -57.2419 & 1.8977 \\ 0.0 & 57.3000 & 0.0 & 0.0 \\ 0.0 & 0.0 & 57.3000 & 0.0 \\ 0.0 & 0.0 & 0.0 & 57.3000 \\ 0.0590 & 0.0 & 0.0 & 0.0 \end{bmatrix}$$

$$D_{ac} = \begin{bmatrix} 0.0 & -0.0315 & 0.0292 \\ 0.0 & -0.0598 & 0.0555 \\ 0.0 & 0.0 & 0.0 \\ 0.0 & 0.0 & 0.0 \\ 0.0 & 0.0 & 0.0 \\ 0.0 & 0.0 & 0.0 \end{bmatrix} \tag{1f}$$

The open-loop lateral-directional properties are defined as follows: $T_{1/2} = 30$ s (spiral mode), $T_R = 0.31$ s (roll mode), and $\omega_{DR} = 4.67$ rad/s and $\zeta_{DR} = 0.15$ (Dutch roll).

Flight Control System Design Methodology

The flight control system for the AIAA Design Challenge[1] is based on an explicit modeling-following design philosophy. The explicit model-following control system structure includes the following major elements: a *maneuver command generator*, a *regulator*, and a *control selector* (see Fig. 1). Design features and methodology for each element of the flight control system are presented in the following sections.

Maneuver Command Generator Design

The task of designing the maneuver command generator (MCG) is one of translating mission-level and flying-quality requirements into representative dynamic elements (i.e., prefilters). The resulting block diagrams become the forward-path model for the explicit model-following control system. At a conceptual level, the aircraft responds like the MCG to pilot commands or commands from a trajectory command generator when the regulator is able to provide good model-following performance. This, in turn, is dependent upon the control mechanization having adequate control power and bandwidth and the aircraft having adequate performance. In addition, the MCG models are designed to accommodate control system and aircraft performance limitations.

The MCG design philosophy that the authors have developed for several programs[2,4–8] provides a methodology for achieving the requisite handling qualities for automated manual flight and good autopilot performance for fully automatic flight. The handling qualities and mission-level requirements are used to define the structure and parameters of the MCG models. The MCG structure includes both control sensitivity and dynamic filter elements. The structure of the MCG model is also driven by a desire to command only variables that are measured or estimated from a standard suite of flight control sensors.

The lateral-directional MCG is designed to provide decoupled control of roll attitude and sideslip. Lateral stick commands roll rate about the velocity vector with roll attitude being held whenever the stick is in detent (i.e., rate command/attitude hold). Decoupling sideslip and the roll rate/attitude responses provide good turn coordination for roll commands and a wing-level sideslip response for pedal inputs. With the wings held level for pedal inputs, small heading changes can be made rapidly with pedal commands (i.e., $\Delta\psi = -\Delta\beta$ for $\phi = 0$). This feature is useful for managing crosswinds close to a runway or for making wing-level azimuth changes for a gunnery task. Good Dutch roll dynamics are also a product of the sideslip model-following structure.

Roll Rate Command

Lateral control sensitivity is defined in terms of the commanded steady-state roll rate to the lateral stick force gradient (i.e., $\Delta P_{ss}/\Delta F_{slat}$). A value of 10 deg/s/lb is selected for the lateral control sensitivity. This is representative of lateral control gradients about the stick centered position. The lateral control gradient would be increased approximately by a factor of 2 for large stick force commands (e.g., beyond 50% of the maximum) to generate the maximum roll rate at reasonable stick force levels. A second-order filter with a zero is used to model the desired roll response, i.e.,

$$\frac{P_{cmd}}{P_{ss}} = \frac{\omega_P^2 \tau_P (s + 1/\tau_P)}{s^2 + 2\zeta_P \omega_P s + \omega_P^2} \tag{2a}$$

where

$$\tau_P = 0.625 t_{90P} \qquad \omega_P = \frac{1.789}{t_{90P}} \qquad \zeta_P = 0.8944 \tag{2b}$$

The parameters of this filter are selected to produce a first-order-like response. The selected value for the rise time is $t_{90P} = 1.0$ s. This rise time produces a response that is similar to a first-order response that has a time constraint $T_R = 0.38$ s. This is well below the 1-s limit as specified within MIL–F–8785C for level 1 flying qualities.

Sideslip Command

Directional control sensitivity is defined as the ratio between sideslip and pedal force (i.e., $\Delta\beta_{ss}/\Delta F_{ped}$). Directional control sensitivity is selected to be 0.25 deg/lb. The sideslip command filter is defined by a second-order transfer function, e.g.,

$$\frac{\beta_{cmd}}{\beta_{ss}} = \frac{\omega_\beta^2}{s^2 + 2\zeta_\beta \omega_\beta s + \omega_\beta^2} \tag{3a}$$

where

$$\omega_\beta = \frac{3.36}{t_{90\beta}} \qquad \zeta_\beta = 0.8944 \tag{3b}$$

For this filter, $t_{90\beta} = 1.12$ s ($\omega_\beta = 3.0$ rad/s). With an explicit model-following control system the parameters of the filter represent the desired Dutch roll dynamics. With $\zeta_\beta = 0.8994$ and $\omega_\beta = 3.0$ rad/s, all Dutch roll requirements for level 1 flying qualities ($\zeta_{DR} > 0.49$, $\zeta_{DR}\omega_{DR} > 0.35$, $\omega_{DR} > 1.0$) are all surpassed by the selected design parameters.

MCG State-Space Model

The above specifications for control sensitivity and the desired dynamic response are used to construct the MCG state-space model. Because of the design requirement to decouple the roll and sideslip

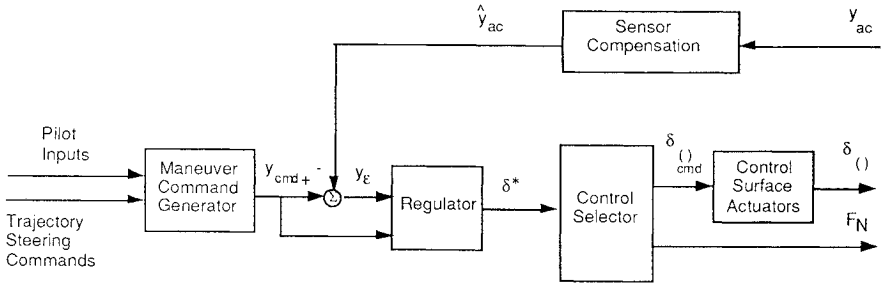

Fig. 1 Flight control structure.

responses, the MCG state-space model comprises two decoupled partitions, one for each response. The state-space model for the lateral-directional MCG is specified as follows:

$$\begin{aligned} \dot{x}_{\text{mcg}} &= A_{\text{mcg}} x_{\text{mcg}} + B_{\text{mcg}} u_{\text{mcg}} \\ y_{\text{mcg}} &= C_{\text{mcg}} x_{\text{mcg}} + D_{\text{mcg}} u_{\text{mcg}} \end{aligned} \tag{4a}$$

where

$$x_{\text{mcg}} = \begin{bmatrix} x_{P1} \\ x_{P2} \\ x_{\phi} \\ x_{\beta 1} \\ x_{\beta 2} \end{bmatrix} = \begin{bmatrix} \text{roll rate filter state 1, deg/s} \\ \text{roll rate filter state 2, deg/s}^2 \\ \text{roll attitude state, deg} \\ \text{sideslip filter state 1, deg} \\ \text{sideslip filter state 2, deg/s} \end{bmatrix} \tag{4b}$$

$$u_{\text{mcg}} = \begin{bmatrix} F_{\text{slat}} \\ F_{\text{ped}} \end{bmatrix} = \begin{bmatrix} \text{lateral stick force, lb} \\ \text{pedal force, lb} \end{bmatrix} \tag{4c}$$

$$y_{\text{mcg}} = \begin{bmatrix} \dot{P}_c \\ P_c \\ \phi_c \\ \dot{\beta}_c \\ \beta_c \end{bmatrix} = \begin{bmatrix} \text{roll acceleration command, deg/s}^2 \\ \text{roll rate command, deg/s} \\ \text{bank angle command, deg} \\ \text{sideslip command, deg/s} \\ \text{sideslip command, deg} \end{bmatrix} \tag{4d}$$

and

$$A_{\text{mcg}} = \begin{bmatrix} -5.3336 & 1.0 & 0.0 & 0.0 & 0.0 \\ -8.8903 & 0.0 & 0.0 & 0.0 & 0.0 \\ 1.0 & 0.0 & 0.0 & 0.0 & 0.0 \\ 0.0 & 0.0 & 0.0 & -5.3664 & 1.0 \\ 0.0 & 0.0 & 0.0 & -9.0000 & 0.0 \end{bmatrix}$$

$$B_{\text{mcg}} = \begin{bmatrix} 33.3388 & 0.0 \\ 88.9034 & 0.0 \\ 0.0 & 0.0 \\ 0.0 & 0.0 \\ 0.0 & 2.25 \end{bmatrix}$$

$$C_{\text{mcg}} = \begin{bmatrix} -5.3336 & 1.0 & 0.0 & 0.0 & 0.0 \\ 1.0 & 0.0 & -0.0018 & 0.0 & 0.0 \\ 0.0 & 0.0 & 1.0 & 0.0 & 0.0 \\ 0.0 & 0.0 & 0.0 & -5.3664 & 1.0 \\ 0.0 & 0.0 & 0.0 & 1.0 & 0.0 \end{bmatrix}$$

$$D_{\text{mcg}} = \begin{bmatrix} 33.3388 & 0.0 \\ 0.0 & 0.0 \\ 0.0 & 0.0 \\ 0.0 & 0.0 \\ 0.0 & 0.0 \end{bmatrix} \tag{4e}$$

Generalized Actuator Design

A key feature of the flight control design approach is the use of generalized controls to represent the physical actuators when the regulator is designed. Our experience has shown that using generalized controls simplifies the control law's complexity[2,5,6] due to the elimination of redundant controls from the control law. Generalized controls serve an essential function when a mixed-sensitivity H_∞ synthesis method is used. For H_∞ synthesis, the regulated variables must be independent and there must be one controller for each regulated variable. The regulated variables for the H_∞ controller are roll rate and sideslip. Thus, only two of the three physical controls (i.e., ailerons, differential horizontal tail, and rudder) can be used. By using generalized controls, these three control surfaces can be represented by a generalized roll acceleration controller and a generalized yaw acceleration controller.

The generalized actuator dynamics are modeled by low-order transfer functions. The form of the transfer function is dependent on the specific design. A second-order representation of the generalized actuator dynamics is required for the regulator synthesis when actuator rate is included as a part of the design problem. Weighting or penalizing actuator rate is one means for achieving realistic multivariable regulator designs. By using a second-order model of the actuator, the actuator rate can be included in the regulator design model without having a direct feed-through term. Synthesis techniques based on the H_∞ norm can handle direct feed-through, whereas those based on H_2 cannot.

As in the case of the AIAA Design Challenge problem,[1] the actuators for the aircraft are already selected. For this case, the generalized actuators must represent the dynamics of the existing actuators. For this design, the generalized actuators are modeled as

$$\begin{aligned} \dot{x}_\delta &= A_\delta x_\delta + B_\delta u_\delta \\ y_\delta &= C_\delta x_\delta + D_\delta u_\delta \end{aligned} \tag{5a}$$

where

$$x_\delta = \begin{bmatrix} x_{\delta_{\dot{P}}} \\ x_{\delta_{\dot{R}}} \end{bmatrix} = \begin{bmatrix} \text{generalized roll acceleration state, \%} \\ \text{generalized yaw acceleration state, \%} \end{bmatrix} \tag{5b}$$

$$u_\delta = \begin{bmatrix} \delta_{\dot{P}_c} \\ \delta_{\dot{R}_c} \end{bmatrix} = \begin{bmatrix} \text{generalized roll acceleration command, \%} \\ \text{generalized yaw acceleration command, \%} \end{bmatrix} \tag{5c}$$

$$y_\delta = \begin{bmatrix} \delta_{\dot{P}} \\ \delta_{\dot{R}} \end{bmatrix} = \begin{bmatrix} \text{generalized roll acceleration command, \%} \\ \text{generalized yaw acceleration command, \%} \end{bmatrix} \tag{5d}$$

and

$$A_\delta = \begin{bmatrix} -20.0 & 0.0 \\ 0.0 & -20.0 \end{bmatrix} \qquad B_\delta = \begin{bmatrix} 20.0 & 0.0 \\ 0.0 & 20.0 \end{bmatrix}$$

$$C_\delta = \begin{bmatrix} 1.0 & 0.0 \\ 0.0 & 1.0 \end{bmatrix} \qquad D_\delta = \begin{bmatrix} 0.0 & 0.0 \\ 0.0 & 0.0 \end{bmatrix} \tag{5e}$$

Each of the two generalized controllers (i.e., roll and yaw acceleration) has an associated control power level. A control distribution matrix (B^*_{AC}) is defined as a diagonal matrix where the diagonal elements represent the maximum control power normalized by 100%; thus, the generalized controls have the units of percentage of maximum control. The maximum control represents, not an actual control limit, but a reasonable level of the available control power that can be achieved in a decoupled manner with an assumed level of deflection from the various physical controllers.

The matrix B^*_{AC} can be determined by knowing the control distribution matrix for the physical controls (B_{AC}) and the allowed excursion for each controller ($\Delta\delta_{\max}$). Here $\Delta\delta_{\max}$ represents the difference between the trim setting and the controller limit or an assumed maximum control deflection. For example, the selected design point represents a high-q flight condition. For this flight condition, it is unreasonable to assume that one would use the complete rudder deflection for controlling the aircraft. Using the procedure described in Ref. 6 and assuming maximum control excursions $\delta_{A,\max} = 5$ deg, $\delta_{D,\max} = 5$ deg, and $\delta_{R,\max} = 10$ deg yield

$$B^*_{AC} = \begin{bmatrix} 0 & \dfrac{Y_{\delta_R}}{N_{\delta_R}} \\ \dfrac{\Delta \dot{P}_{\max}}{100\%} & 0 \\ 0 & \dfrac{\Delta \dot{R}_{\max}}{100\%} \end{bmatrix} = \begin{bmatrix} 0 & -0.0985 \\ 0.0672 & 0 \\ 0 & 0.0153 \end{bmatrix} \tag{6}$$

The off-diagonal term that defines a side acceleration due to generalized yaw acceleration is included because the study aircraft does not have the ability to produce a yawing moment with zero side force.

Regulator Synthesis Approaches

The regulator design strategy is to use two different methods and conduct comparison studies of the different regulators. Both LQR and H_∞ mixed-sensitivity regulators are designed. The following briefly describes the regulator design methodologies.

LQR Synthesis

The LQR regulator gain synthesis process includes several steps. The first step involves solving for the state feedback gain matrix using a steady-state solution of the Riccati equation to minimize a quadratic performance index. The next step involves transforming the state feedback control law to an output feedback control law where the outputs are aircraft sensor measurements. The final step involves simplifying the control law by removing insignificant gains.

The basis of the LQR method is that a control system is designed that is optimal relative to a performance index that is a quadratic function of the outputs and inputs. This performance index takes the form

$$J = \int_0^\infty [y'Qy + u'Ru]\,dt \tag{7}$$

By doing this, the designer can directly relate Q to those quantities that are of interest (i.e., tracking errors, control actuator rates, and control deflection magnitudes). Computer-aided design packages such as Matrix$_x$ and MATLAB provide functions for solving this formulation of the linear quadratic regulator problem.

The regulator synthesis process is based on selecting values for the output weighting and control usage performance indices Q and R. For the tracking problem, as characterized by the model-following control system structure depicted in Fig. 1, proportional and integral tracking errors and control surface displacement are weighted. All other diagonal terms (e.g., aircraft response variables and the MCG commands) are set to zero. Initial selection of the nonzero Q_{ii} and R_{ii} terms can be based on something like Bryson's rule, i.e., $Q_{ii} = 1/y_{ii}^2$ (e.g., $1/P_{\varepsilon_{\max}}^2$) and $R_{ii} = 1/u_{ii}^2$ (e.g., $1/\delta_{P_{\max}}^2$). When the design model includes other control terms besides the generalized controls (e.g., MCG commands and gust inputs), the R_{ii} that correspond to these terms must be set to very large values. By doing this, these inputs are effectively eliminated from the control law solution. As a test, the R_{ii} terms associated with the MCG inputs need to be large enough such that the closed- and open-loop eigenvalues of the MCG state-space model are the same.

Selection of diagonal elements of Q and R is an iterative process. The first design goal is to select values for Q_{ii} and R_{ii} that yield good model-following performance and disturbance rejection. Increasing values for the Q_{ii} elements (i.e., higher penalty on tracking errors) and reducing the values of the R_{ii} elements (i.e., increased control authority) improve tracking performance and increase control bandwidth. After good tracking performance, disturbance rejection, and response decoupling are achieved, the control surface rate can be penalized to reduce the high-frequency control activity. Frequency responses of the generalized controls are a good means for assessing high-frequency control activity.

The final choices for the output and control performance indices Q and R are specified below along with a specification for the weighting matrix W, which is used to transform the state feedback control law to an output feedback control law:

$$y = \left[y_{ac} : y_\delta : y_{\text{mcg}} : P_\varepsilon, \phi_\varepsilon, \dot{\beta}_\varepsilon, \beta_\varepsilon, \int \phi_\varepsilon, \int \beta_\varepsilon\right]^T$$

$$Q_{ii} = [\text{zeros}(1,5) : 0.05, 0.05 : \text{zeros}(1,5) : 4,$$
$$25, 20, 100, 200, 500] \tag{8}$$

$$W_{ii} = [10^{-6}\ \text{ones}(1,6)\ \text{ones}(1,13)]$$

$$u = [\delta_{\dot{P}_c}, \delta_{\dot{R}_c}, F_{\text{slat}}, F_{\text{ped}}, \nu_g]$$

$$R_{ii} = [0.05, 0.05, 10^6 \text{ones}(1,3)]$$

As a part of the regulator synthesis process, the state feedback control law, which is generated from the LQR solution, is converted to an output control law by a transformation that maintains the eigenvalues of the closed-loop system.[2] This step is useful in that the engineering interpretation of the resulting LQR gain synthesis process is often enhanced by having an output gain solution. This transformation can be made whenever the output vector of the system model that is used for the LQR synthesis provides observability for all of the system's state variables and has at least as many output elements as there are state variables.[2]

H_∞ Regulator Synthesis

The H_∞ regulator synthesis procedure used a mixed-sensitivity approach. The problem is as shown in Fig. 2. The closed-loop transfer function matrix in this case is

$$H_{zw} = \begin{bmatrix} W_1 S \\ W_2 T \end{bmatrix} \tag{9}$$

where $S(s) = [I + G(s)K(s)]^{-1}$ is the system *sensitivity function* and $T(s) = I - S(s)$ is the *complementary sensitivity function*. The closed-loop transfer function matrix $H_{zw}(s)$ contains weighting filters $W_1(s)$ and $W_2(s)$, which are chosen to simultaneously shape $S(s)$ and $T(s)$, respectively, resulting in the mixed-sensitivity design.

The complementary sensitivity weighting function $W_2(s)$ is chosen based on the frequency-dependent complex uncertainties translated to the output. The complementary sensitivity weighting function is chosen to be larger than the sensor uncertainty to ensure the stability of the H_∞ mixed-sensitivity controller with respect to the unstructured uncertainties. Iterations are carried out until the complementary sensitivity function singular values reach their specification. An initial candidate design is then identified. An alternative strategy proposed by Safonov[7,9] is to choose $W_2^{-1}(s)$ so as to specify the desired roll-off rates.

The complementary weighting filter $W_2(s)$ was chosen to be

$$W_2 = 10\frac{s + 0.1}{s + 1000} I_2 \tag{10}$$

based on the uncertainty assumed for the sensor time delay (Table 1). It is shown as a dashed line in Fig. 3. The sensitivity weighting filter $W_1(s)$ was chosen to be compatible with $W_2(s)$, and several values of γ were tried, with $\gamma = 0.1$ being chosen to meet the tracking specification. The sensitivity weighting filter $W_1(s)$ is also shown as a dashed line in Fig. 3 and is defined as

$$W_1 = \gamma\frac{s + 100}{s + 0.01} I_2 \tag{11}$$

The resulting sensitivity and complementary sensitivity functions for the H_∞ controller are as shown in Fig. 3 (solid lines). The smooth shapes of the functions and the fact that they are below the acceptable bounds indicate an acceptable feedback regulator design.

Control Selector Design

The control selector provides the controller mechanization function of the flight control system (see Fig. 1). The primary function

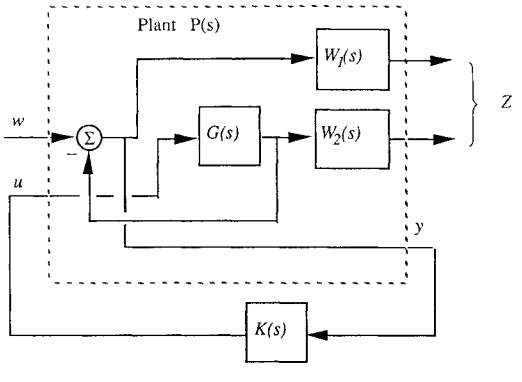

Fig. 2 Mixed-sensitivity diagram.

Table 1 Sensor uncertainty model

Description	Scaling factor
Roll rate sensor time delay, 20 ms	$\frac{600s}{s^2 + 300s + 30{,}000}$
Sideslip sensor time delay, 20 ms	$\frac{600s}{s^2 + 300s + 30{,}000}$

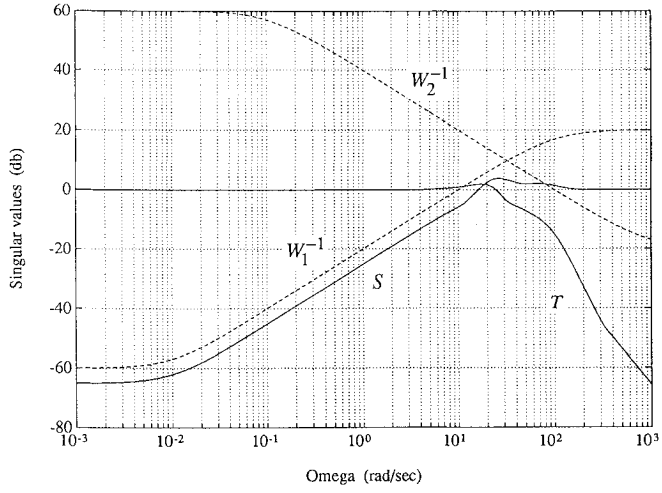

Fig. 3 H_∞ mixed-sensitivity design verification.

of the control selector is to transform the generalized control commands, which are generated by the flight control system regulator, to commands for the aircraft's control surface actuators and the propulsion control system. The design requirement for this transformation is to match the loop gain of the flight control system with physical actuators with the closed-loop system based on generalized controls.[2,6]

The control transformation is based on solving for a pseudoinverse. The following equation defines this transformation:

$$\delta_c = T\delta_c^* \tag{12}$$

where

$$T = N_{\max}(B_{AC}N_{\max})^{\#}B_{AC}^*$$

Here $(B_{AC}N_{\max})^{\#}$ is the pseudoinverse of the control distribution matrix for the physical controls (B_{AC}), B_{AC}^* is the control distribution matrix for the generalized controls [see Eq. (6)], and $N_{\max}$ is a normalization matrix for the pseudoinverse computation. For the values of B_{AC} and B_{AC}^* that were defined earlier in the paper and for $N_{\max} = \text{diag}([5, 5, 10])$ the control selector transformation matrix is defined as

$$T = \begin{bmatrix} 0.0167 & 0.0014 \\ 0.0500 & 0.0043 \\ 0.0538 & -0.1000 \end{bmatrix} \tag{13}$$

By solving for the control transformation on-line, gain scheduling, as required by changes in control power and the relative importance of various redundant controls, is automatically accommodated. For the DMICS design,[2] this alone handled the control law gain-scheduling requirements for changes in Mach number and altitude. This allowed a constant set of regular gains to be used.

Flight Control System Design Comparison

The goal of this section is to illustrate the differences and similarities of the LQR and H_∞ synthesis through a number of comparisons. First, the structures of the two regulators are compared. Next, the model-following accuracy for the two approaches is compared. This is followed by comparisons of the transient performance. The next comparisons address stability and performance robustness. The final comparison looks at the effectiveness of the control laws to suppress a lateral gust disturbance.

Regulator Structure

The structures and gains for the LQR and H_∞ control laws are presented in Fig. 4. Features of each control law are described below.

Aside from the frequency shaping that results from the closure around the open-loop generalized actuators, the LQR control law is a static compensator with feedforward, proportional error, and integral error components. Integral error control is implemented explicitly so that special-purpose logic can be added to the integrators (e.g., integrator anti-windup). Individual elements of the three gain sets ($K_{y,FF}$, $K_{y,FB}$, and $K_{y,IE}$) can be implemented as in-line code to improve the control law's real-time performance. Individual gain elements can also be gain scheduled if necessary.

The mixed-sensitivity H_∞ control design usually results in controllers with very fast poles. The fast poles are generally due to the lead-lag shapes of the chosen weighting filters. Since it is impractical to implement these high-frequency elements, the controller's order must be reduced. Several different controller reduction methods have been used. This turns out to be a very delicate problem. The singular perturbation controller model order reduction yields the best results, and the more sophisticated model order reduction methods seem to be totally unsatisfactory. This is due to the fine cancellations that occur in the mixed-sensitivity method.[10]

Initially an eighth-order controller was obtained from the mixed-sensitivity design. After controller model order reduction, a sixth-order controller was obtained. This controller is implemented as a sixth-order state-space model, as shown in the lower part of Fig. 4. Even this reduced-order controller has relatively fast dynamics (i.e., $\omega = 111.6$ rad/s).

Model-Following Performance

Model-following performance is evaluated by comparing the frequency responses of the MCG and the two control law designs to lateral stick and pedal commands. Figure 5 presents the frequency responses for a lateral stick command. Looking at both the magnitude and phase responses, it can be seen that the LQR and H_∞ control law designs achieve excellent model-following performance up to 10 rad/s. The primary difference between the two controllers is that the H_∞ design has more high-frequency roll-off due to its higher order structure.

Transient Performance

The transient responses were obtained from a simulation model that has linear aircraft dynamics and nonlinear actuator dynamics. The actuator model implemented both the position and rate limits. The aircraft state-space model included the effects of the product of inertia (I_{XZ}) in its terms.

The transient responses for both controllers are good. Both use reasonable control effort and provide good tracking properties. Examining transients due to the lateral stick input in Fig. 6, we note that both controllers produce similar results, with the H_∞ design providing slightly better suppression of the sideslip response. However, both controller provide excellent turn coordination. Examining the transient responses due to the pedal input in Fig. 7, we note that the H_∞ controller has better initial tracking properties for sideslip, but it does not exhibit the roll attitude hold feature of the LQR design.

Stability and Performance Robustness

The robustness analysis is a key step in the evaluation procedure. The stability and performance robustness of the design is evaluated through construction of the interconnection structure of the plant and its uncertainties. All uncertainties are normalized. The total uncertainty is isolated in the form of the standard M-Δ diagram.[7] Structured singular values are computed for both stability and performance robustness.

The stability robustness evaluation procedure is as follows. The controllers are tested for robustness with respect to all the *real* parameter uncertainties that occur in the feedback loop. If the design is robust with respect to the real parameter perturbations (i.e., the structured singular value remains below unity for all frequencies), then the evaluation moves to the next step. Otherwise, the worst-case design modeling technique[7,8] is employed to incorporate all the real parameter uncertainties in the design until a feedback controller is

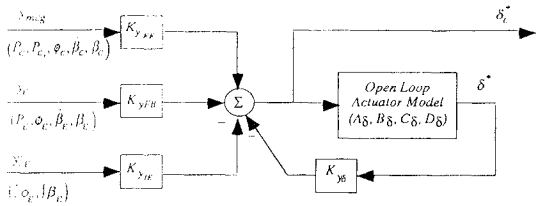

$$K_{yFF} = \begin{bmatrix} -0.5919 & -1.8418 & 0.0440 & -3.5557 & -57.4517 \\ 0 & 0 & 0 & -2.5797 & -5.7576 \end{bmatrix} \quad K_{yFB} = \begin{bmatrix} -9.7488 & -44.4328 & 1.1235 & 47.7742 \\ -1.2686 & -6.1238 & 21.3541 & 80.0546 \end{bmatrix}$$

$$K_{yIE} = \begin{bmatrix} -62.6952 & 0 \\ 0 & 99.1289 \end{bmatrix} \quad K_{y\delta} = \begin{bmatrix} 1.3407 & 0 \\ 0 & 3.4315 \end{bmatrix}$$

a) LQR control law

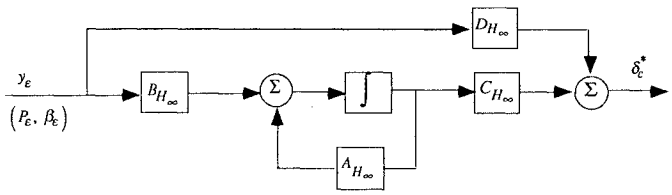

$$A_{H_\infty} = \begin{bmatrix} -0.0015 & 0 & 0 & 0 & 0 & 0 \\ 0 & -0.0100 & 0 & 0 & 0 & 0 \\ 0 & 0 & -0.0100 & 0 & 0 & 0 \\ 0 & 0 & 0 & -100.7559 & 0 & 0 \\ 0 & 0 & 0 & 0 & -61.9249 & 92.8763 \\ 0 & 0 & 0 & 0 & -92.8763 & -61.9249 \end{bmatrix}$$

$$B_{H_\infty} = \begin{bmatrix} 2.9677e{+}02 & -2.6251e{+}00 \\ 3.3242e{+}02 & -2.1776e{+}03 \\ -4.4855e{+}02 & 9.1857e{+}02 \\ 1.2087e{+}01 & -1.9300e{+}05 \\ -6.8666e{+}00 & 1.9271e{+}05 \\ -1.2367e{+}02 & 1.3061e{+}05 \end{bmatrix} \quad D_{H_\infty} = \begin{bmatrix} 6.7200 & -0.0105 \\ -0.1581 & -0.0001 \end{bmatrix}$$

$$C_{H_\infty} = \begin{bmatrix} -0.1797 & -0.3825 & -0.4438 & 0.0228 & 0.0302 & -0.0142 \\ 0.3232 & 0.3722 & 0.4815 & 5.3188 & 2.7618 & -6.1169 \end{bmatrix}$$

b) H_∞ control law

Fig. 4 Comparison of LQR and H_∞ control law structures.

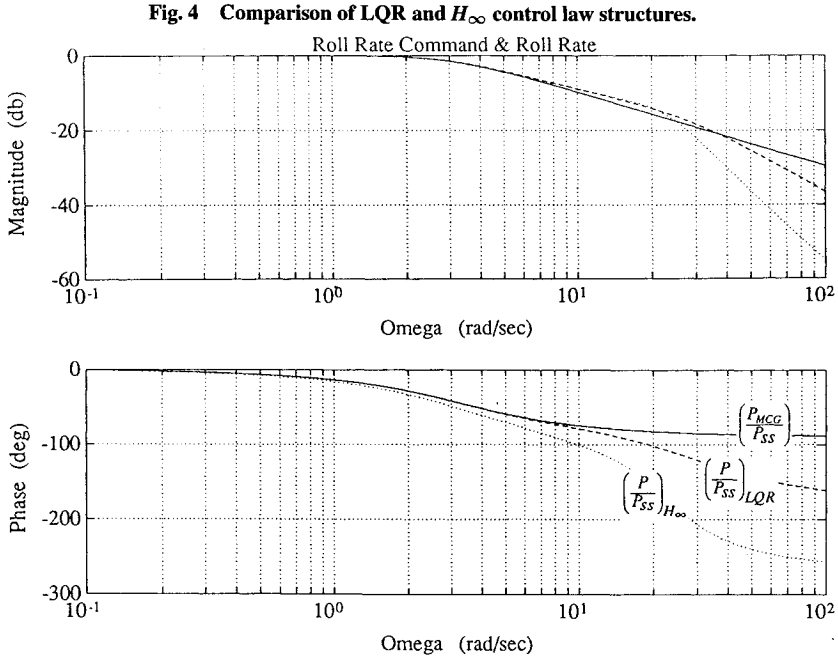

Fig. 5 Comparison of roll rate model-following performance.

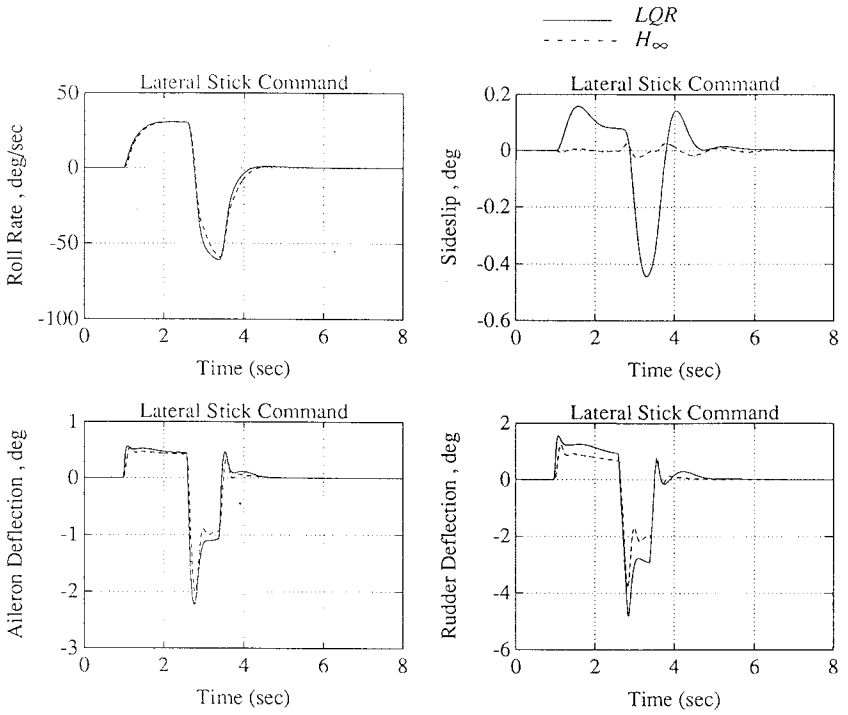

Fig. 6 Comparison of roll tracking performance: lateral stick command.

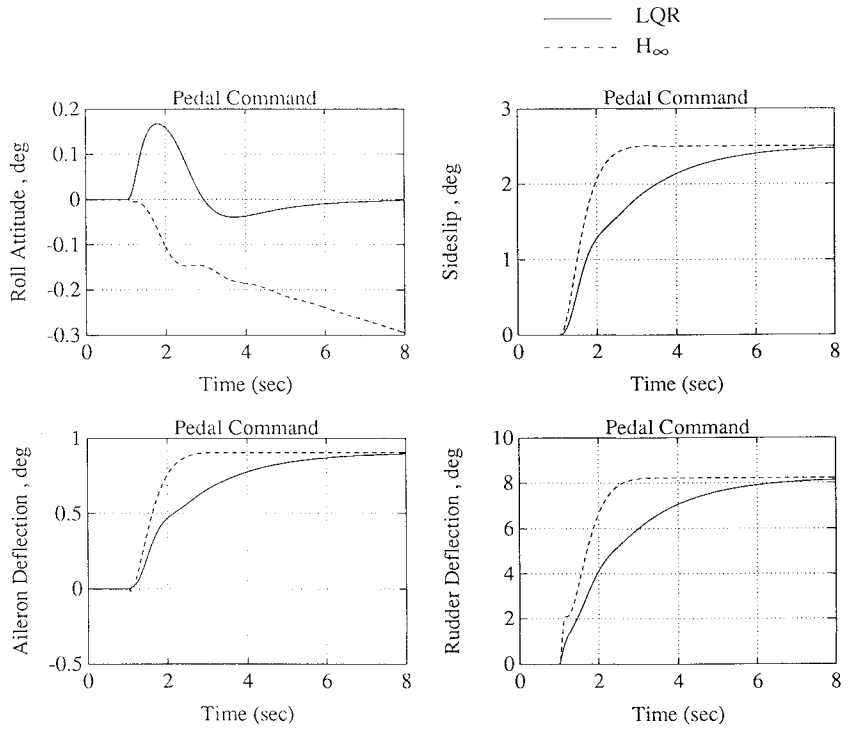

Fig. 7 Comparison of sideslip tracking performance: pedal force command.

found that is robust with respect to all parameter uncertainties. Both the LQR and H_∞ designs did not require this redesign step.

The last step in the robustness testing is the overall performance robustness evaluation. The structured singular value is plotted with the inclusion of all modeling uncertainties that occur in the system. This encompasses *all* real and complex uncertainties evaluation *as well as* the fictitious uncertainty due to the transient response performance. The evaluation is complete once this performance robustness structured singular value remains below unity for all frequencies. In that case, both robust stability and performance are ensured with respect to the class of modeling errors considered.

Selected uncertainties were chosen from a representative uncertainty model data base to determine the stability and performance robustness of the two controller designs. The selected uncertainties include the sensor time delays, which were specified in Table 1, and the six aerodynamic model uncertainties that are listed in Table 2. The last entry in Table 2 defines a model for testing performance robustness. All of the uncertainties are 1×1 blocks.

The structured singular values for each design are computed with all nine uncertainty sources listed in Tables 1 and 2. The resulting combined stability and performance structured singular values for each design are compared in Fig. 8. As shown, the peak structured

Table 2 Selected uncertainty sources

Description	Scaling factor
ΔC_{y_β}	14%
ΔC_{l_P}	28%
ΔC_{l_R}	20%
ΔC_{n_β}	30%
ΔC_{n_P}	200%
$\Delta C_{n_{\delta R}}$	12.5%
Performance	$1/(s+0.1)$

Table 3 Turbulence response comparison

Response variable	RMS response to lateral gust		
	LQR	H_∞	Open loop
n_y	0.18	1.00	0.22
P	0.21	1.00	4.29
R	0.36	1.00	0.55
β	1.53	1.00	2.48
δ_A	0.58	1.00	
δ_D	0.57	1.00	
δ_R	0.10	1.00	

Note: All responses are normalized by the H_∞ RMS response.

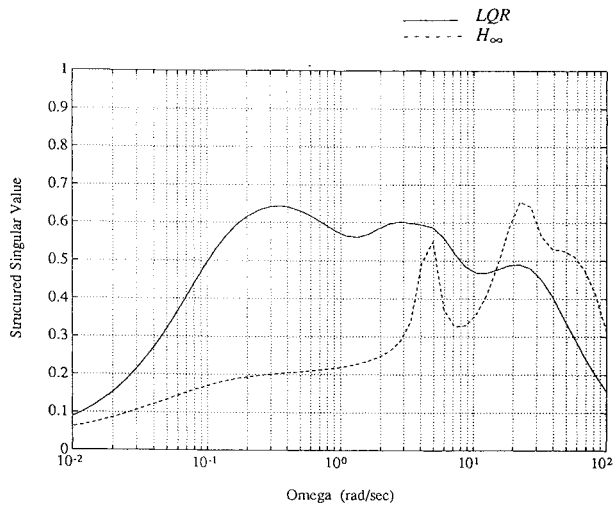

Fig. 8 Comparison of combined stability and performance robustness.

singular values for each design are well below the unity threshold, thus indicating that the closed-loop system has both robust stability and performance. The maximum structured values for each design are nearly identical in magnitude. Thus, both the LQR and the H_∞ designs would seem to have comparable levels of robust stability and performance.

Disturbance Rejection

Finally, Table 3 compares the root-mean-square (RMS) values of the two controllers. The LQR controller generally outperforms the H_∞ controller as far as RMS responses to turbulence is concerned. However, the H_∞ controller has a better sideslip RMS response but also uses more control power in an RMS sense.

Conclusion

This paper has presented a design approach that is responsive to the AIAA Flight Control Design Challenge problem. An explicit model-following control structure was selected and two different regulator design approaches were evaluated. Designs and evaluation results for a lateral-directional point design were presented. A new H_∞ synthesis procedure has been presented suitable for application to practical control problems. The innovative part of this synthesis procedure is the separation of feedback and feedforward designs as well as a methodology for a systematic evaluation of the designs robustness to design model uncertainty.

For this example, both synthesis approaches yield acceptable performance. The H_∞ techniques have provided a theoretically sound approach to robust control design. They have the ability to deal with various sources of modeling error and can treat performance requirements in the frequency domain. All computations can be performed in terms of state-space formulations. However, there is not a "Bryson's rule" for H_∞ control design, and it may take some effort to generate an initial design. Controller model order reduction is required for the H_∞ design, and this proved to be a delicate numerical problem. Generic cancellations in the mixed-sensitivity method may give rise to lack of robustness with respect to variations in some stability derivatives.

Both designs demonstrated excellent model-following performance. The H_∞ controller shows slightly better sideslip suppression for roll commands (i.e., turn coordination), better sideslip tracking for pedal commands, but no roll attitude hold for the sideslip command. Both designs proved to have adequate stability and performance robustness. Finally, the LQR-based controller demonstrated better gust rejection properties (i.e., lower RMS disturbance with less control activity). For the lateral acceleration n_y and yaw rate R responses, the RMS response for the H_∞ control law actually exceeded the open-loop values.

The primary difference between the control laws produced by the two design techniques pertains to their control law structures. The LQR control law produces a simpler control law. Its structure can be implemented with in-line code, and gain scheduling is straightforward. Integrators for the integral error control are also implemented separately, thus permitting incorporation of explicit logic to control integrator windup. The H_∞ is a high-order dynamic compensator with large numerical variation in the elements of its compensator matrices. This wide variation in numeric values could dictate usage of increased precision numerical representations for the controller's implementation. Increased numerical precision requires more memory and computer cycle time for each computation. Another implementation concern deals with the high-frequency dynamics of the H_∞ controller. The high-frequency dynamics could unduly increase the required iteration rate for the control law.

References

[1]Duke, L., AIAA Controls Design Challenge Announcement, 1990.

[2]Shaw, P. D., Haiges, K. R., Rock, S. M., Vincent, J. H., Emami-Naeini, A., Anex, R. A., Fisk, W. S., and Berg, D. F., "Design Methods for Integrated Control Systems," AFWAL-TR-88-2061, June 1988.

[3]Vincent, J. H., and Haiges, K. R., "Use of Explicit Model-Following for Direct Incorporation of Flying Quality Design Requirements," AIAA Paper 87-2254, Aug. 1987.

[4]Vincent, J. H., "Direct Incorporation of Flying Qualities Criteria into Multivariable Flight Control Design," AIAA Paper 84-1830, Aug. 1984.

[5]Vincent, J. H., "Application of Modern Control Design Methodologies to Oblique Wing Research Aircraft," Systems Control Technology, SCT Report No. 4520-280-1, July 1991.

[6]Vincent, J. H., and Anex, R. A., "Flight Control Design Considerations for STOL Powered-Lift Flight," AIAA Paper 90-3225, Sept. 1990.

[7]Haiges, K. R., Chiang, R. Y., Madden, K. P., Emami-Naeini, A., Anderson, M. R., and Safonov, M. G., "Robust Control Law Development for Modern Aerospace Vehicles," WL-TR-91-3105, Aug. 1991.

[8]Anderson, M. R., Emami-Naeini, A., and Vincent, J. H., "Robust Control Law Development for a Hypersonic Cruise Vehicle," *Proceedings of the Automatic Control Conference*, June 1991.

[9]Chiang, R. Y., Safonov, M. G., and Tekway, J. A., "$H\infty$ Flight Control Design with Large Parametric Robustness," in *Proceedings of the American Control Conference*, San Diego, May 1990.

[10]Doyle, J. C., Glover, K., Khargonekar, P. K., and Francis, B., "State-Space Solutions to Standard H_2 and H_∞ Control Problems," *IEEE Transactions on Automatic Control*, Vol. AC-34, No. 8, 1989, pp. 831–847.

[11]Jones, R. D., "Structured Singular Value Analysis for Real Parameter Variations," *Proceedings of the AIAA Guidance, Navigation, and Control Conference* (Monterey, CA), AIAA, Washington, DC, 1987, pp. 1424–1432.

[12]Osborne, E. E., "On Pre-Conditioning of Matrices," *Journal of the Association for Computing Machinery*, Vol. 7, 1960, pp. 338–345.

[13]Khraishi, N. M., and Emami-Naeini, A., "A Characterization of Optimal Scaling for Structured Singular Value Computation," *Systems & Control Letters*, Vol. 15, 1990, pp. 105–109.

[14]Sefton, J., and Glover, K., "Pole/Zero Cancellations in the General H_∞ Problem with Reference to a Two Block Design," *Systems & Control Letters*, Vol. 14, No. 4, 1990, pp. 295–306.